A quantum explanation of the magnetic properties of Mn-doped graphene*

Lei Tian-Min(雷天民)[a)†], Liu Jia-Jia(刘佳佳)[a)], Zhang Yu-Ming(张玉明)[b)], Guo Hui(郭 辉)[b)], and Zhang Zhi-Yong(张志勇)[c)]

[a)] *School of Advanced Materials and Nanotechnology, Xidian University, Xi'an* 710071, *China*
[b)] *School of Microelectronics, Xidian University, Xi'an* 710071, *China*
[c)] *School of Information Technology, Northwest University, Xi'an* 710069, *China*

(Received 12 March 2013; revised manuscript received 24 June 2013)

Mn-doped graphene is investigated using first-principles calculations based on the density functional theory (DFT). The magnetic moment is calculated for systems of various sizes, and the atomic populations and the density of states (DOS) are analyzed in detail. It is found that Mn doped graphene-based diluted magnetic semiconductors (DMS) have strong ferromagnetic properties, the impurity concentration influences the value of the magnetic moment, and the magnetic moment of the 8×8 supercell is greatest for a single impurity. The graphene containing two Mn atoms together is more stable in the 7×7 supercell. The analysis of the total DOS and partial density of states (PDOS) indicates that the magnetic properties of doped graphene originate from the p–d exchange, and the magnetism is given a simple quantum explanation using the Ruderman–Kittel–Kasuya–Yosida (RKKY) exchange theory.

Keywords: graphene, first-principles calculation, doping, ferromagnetic properties

PACS: 75.25.–j, 74.25.Ha, 71.20.–b **DOI:** 10.1088/1674-1056/22/11/117502

1. Introduction

Graphene has many outstanding properties including high chemical and thermal stability, high electrical conductivity, and high mechanical strength,[1] so it has attracted extensive research since its discovery in 2004 by Geim and Novoselov.[2–4] An increasing number of papers have reported on the magnetism of molecules or metal atoms adsorbed on graphene[5–9] in recent years; we pay more attention to the magnetic properties of doped graphene-based diluted magnetic semiconductors (DMS). DMS can use both the charge and spin of the electron for a remarkable new generation of nanoscale micro-electronic devices that could be used for information processing and storage.[10] For example, the graphene defect-adsorption of transition-metal (TM) atoms circumvents the problem of TM clustering in favor of efficient hydrogen storage in nanostructured systems.[11] Boron nitride nanoribbons with one substitutional Mn impurity reveal transfer characteristics suitable for a spin current switch, and the system with two Mn impurities behaves as an efficient spin-filter device.[12] The key lab of MEMS of the Ministry of Education in Southeast University proved that gold-doped zigzag graphene nanoribbons in a divacancy could modulate the magnetism and band structure.[13] Eelbo *et al.* investigated the electronic and magnetic properties of single Fe, Co, and Ni atoms and clusters on monolayer graphene on SiC (0001) and found that an increasing Ni cluster size leads to sizable magnetic moments.[14] Since intrinsic graphene has no magnetism, we dope substitutional Mn atoms in the supercells to generate and modify diluted magnetic properties of graphene material. We construct the supercell models of graphene with different impurity concentrations, calculate the magnetic moment, and analyze the atomic populations, the total density of states, (DOS) and partial density of states (PDOS) to develop an explanation of the spin exchange mechanism.

2. Computational methods

Graphene is a two-dimensional (2D) monolayer of carbon atoms tightly packed in a hexagonal crystal lattice.[15] In order to avoid the spurious interactions between periodic images of the graphene layers, the size of the supercells perpendicular to the plane is 15 Å. For Mn-doped graphene, structure optimizations are first performed and then the magnetism calculations are carried out using density functional theory (DFT)[16,17] based on the pseudo-potential technology. The generalized-gradient approximation (GGA) function with the Perdew–Burke–Ernzerhof (PBE) correction[18] is used to obtain stable structural cells. All the crystal structures are fully relaxed via geometrical optimization using the Broyden–Fletcher–Goldfarb–Shanno (BFGS) scheme.[19] The projector augmented wave (PAW)[20,21] simulates the electron–ion interaction. With a cutoff energy of 400 eV, all the supercell structures are optimized until forces in all directions are smaller than 0.05 eV·Å^{-1}. The graphene initial cell in the A, B base vector direction is extended 4–8 units to obtain various super-

*Project supported by the National Science and Technology Major Project of the Ministry of Science and Technology of China (Grant No. 2011ZX02707).
†Corresponding author. E-mail: tmlei@mail.xidian.edu.cn
© 2013 Chinese Physical Society and IOP Publishing Ltd

cell sizes. The 8×8 supercell is shown in Fig. 1(a), and the Mn substitution in the C sites leads to different impurity concentrations.

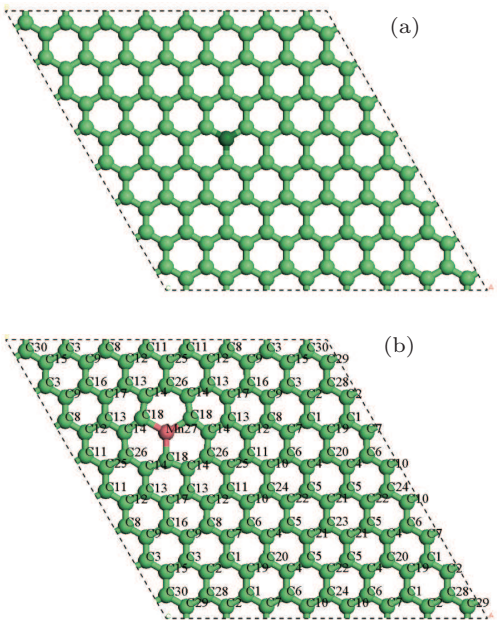


Fig. 1. (color online) The typical structures of (a) the intrinsic 8×8 graphene and (b) corresponding Mn-doped graphene after optimizations. Light green and green spheres represent C atoms, and the green C sites are the possible substitutional positions of Mn atoms. The light red sphere represents an Mn atom.

3. Results and discussion

As shown in Fig. 1(b), the Mn atoms are all seated in the upper center from the center of the hexagonal lattice after structural optimization for five different supercells with a single impurity. According to the first-principles magnetic calculations, the carbon atoms are polarized by the manganese atom to varying degrees, obtaining the different C atoms. So the 8×8 doped supercell consists of C1–C26, Mn27, and C28–C30 in Fig. 1(b), and the atom with the same label possesses the same properties. The atomic Mulliken populations, magnetic moments, and Mn–C distances of graphene-based supercells are shown in Table 1. There is an initial spin of $1.0\mu_B$ in these systems. So they have ferromagnetic properties, as seen from the total magnetic moments. The Mn-doped armchair graphene ribbon has the same ferromagnetic property as these Mn-doped supercells.[22] References [23] and [24] indicate that the substitutional Mn-doped defect in graphene is magnetic in both cases. It is thus clear that an Mn impurity induces the expected magnetic moment. In a further investigation, it is found that the total magnetic moment of Mn-doped graphene varies with the impurity concentration. The 8×8 supercell has the highest magnetic moment of $4.8\mu_B$ while the 4×4 supercell has the lowest magnetic moment of $2.6\mu_B$ among these supercells. The electron configuration of an isolated Mn atom is $(Ar)3d^54s^2$ of 3 unfilled holes with a magnetic spin moment equivalent to 3 spins or $m_s = 3\mu_B$ according to Hund's rules. Including the orbital moment, the moment per Mn atom is estimated from Hund's rules, maximizing $S = 5/2$, $L = 0$, and $J = 5/2$. Note $J = L+S$ for a shell that is more than half filled. The magnetic moment m_{J_z} is the d shell moment expected for an Mn atom with Hund's rules ground states and occupation of the lowest state $J_z = -J$, $m_{J_z} = g_J J\mu_B$, where g_J is the Landé g factor given by the equation

$$g_J = 1 + \frac{J(J+1)+S(S+1)-L(L+1)}{2J(J+1)}, \qquad (1)$$

and $m_{J_z} = 5\mu_B$ is obtained. So the 5×5, 6×6, and 8×8 Mn-doped graphene supercells all have total magnetic moments close to $5.0\mu_B$. As for the other two supercells, the total magnetic moment is near $3.0\mu_B$, consistent with the spin moment in the previous reports.[23,24] A magnetic order occurs, in most instances, in materials with partially filled d or f shells. However, there are magnetic carbon atoms induced by Mn impurities in Mn-doped graphene. The total magnetic moment is always smaller than the moment associated with the pure Mn metal and significant weakening contributions come from the neighboring carbon atoms. The total magnetic moment is big or small depending on the magnetism contribution of Mn and C atoms' exchanges. It is clear that the Mn atomic magnetic moments in the 4×4 and 7×7 doped graphene are only $0.44\mu_B$ and $0.34\mu_B$ while the magnetic moments of the neighboring C atoms are all small. However, other supercells not only have greater magnetic moments of Mn atoms but also have greater magnetic moments of the three nearest C atoms and the three third-nearest C atoms (similar to C18 and C26 sites in Fig. 1(b)), which is opposite to the 4×4 and 7×7 supercells. The spin direction is arranged in spin-up and spin-down with the Mn atom as the center, in agreement with the result that the three nearest C atoms are polarized antiparallel to the magnetic moment of the Mn atom,[23] which brings about the slightly smaller total moment. The nearer the C atoms to the Mn atom, the stronger the exchange. It follows that the polarizations of the electrons are as illustrated in Fig. 2(a). The stronger the polarizations, the darker the arrows. The farther gray arrows stand for the weaker exchange interactions. Figure 2(b) displays the spin density of the 8×8 doped graphene and further indicates the spin arrangement. The spin density overlaps between Mn27 and C18, and the light red spin density of the spin-up Mn27 is hardly distinct. The spin densities of the C18, C14, and C26 are light green, light red, and light green, respectively, very consistent with the atomic moments of C_{first}, C_{second}, and C_{third}. There is only one C23 in the supercell, a special atom because it has the same distance to the three Mn atoms from C23 in the periodic structure. So the C23 of bigger spin density is a little more strongly spin-polarized.

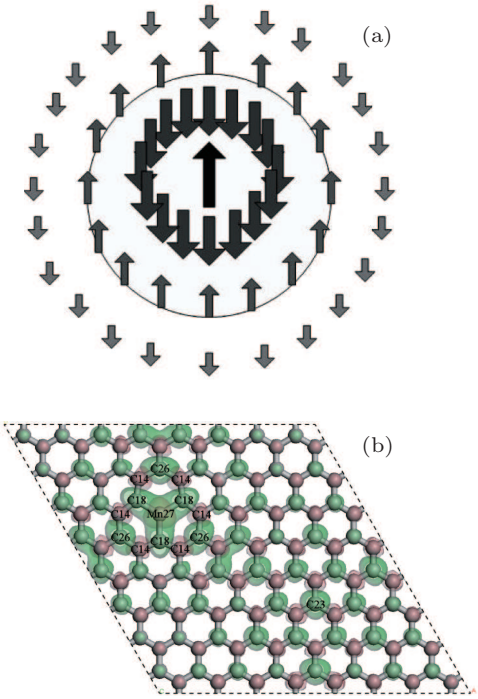


Fig. 2. (color online) (a) Polarization arrangement and (b) spin density. Light red and light green densities are for spin-up and spin-down, respectively, and the isovalue is $1.2648\times10^{-3}e$.

For population analysis, it is widely accepted that the absolute magnitudes of the atomic charge have little physical meaning, since they display a high degree of sensitivity to the atomic basis set with which they are calculated. However, the consideration of the relative values can yield useful information, provided a consistent basis set is used for the calculation. So by comparing the intrinsic Mn cell with the doped supercells, it is obtained how the s, p, and d orbital electrons vary, the same as for the C atoms. The Mn-s and Mn-p orbits lose different quantities of electrons in the doped supercells, while the Mn-d orbit gains a few or is nearly unchanged. It is this change that leads to the total magnetic moment of smaller than $3.00\mu_B$ or $5.00\mu_B$ and gives rise to the Mn atomic moment of less than $3.00\mu_B$, a tiny value. Relatively speaking, the greater the charge or the fewer the total electrons, the smaller the magnetic moment. According to the bond populations, the Mn atoms and the C_{first} with the distance of approximately 1.7 Å form the bonding states, while the Mn atoms and the C_{second}, C_{third} far away from the magnetic atom up to 2.6 Å and 2.9 Å, form anti-bonding orbitals, needing more energy to bond.

Table 1. Atomic populations, atomic magnetic moment (M), total magnetic moment (M_{Total}), and Mn–C distance (D_{Mn-C}) of different supercells of a single impurity. Here C_{first}, C_{second}, and C_{third} are the nearest C atoms, the second nearest C atoms, and the third nearest C atoms to the Mn atom, respectively (similar to C18, C14, and C26 sites in Fig. 1(b)).

Atom	s	p	d	Total	Charge/e	M/μ_B	D_{Mn-C}/Å
The intrinsic cell							
Mn	0.54	0.70	5.76	7.00	0.00		
C	1.05	2.95	0.00	4.00	0.00		
Supercell 4×4	$M_{Total}=2.63\mu_B$						
Mn	0.17	–0.71	5.77	5.23	1.77	0.44	
C_{first}	1.17	3.14	0.00	4.32	–0.32	–0.08	1.71
C_{second}	1.06	3.02	0.00	4.08	–0.08	0.12	2.55
C_{third}	1.04	3.05	0.00	4.09	–0.09	–0.02	2.87
Supercell 5×5	$M_{Total}=4.64\mu_B$						
Mn	0.18	–0.71	5.86	5.33	1.67	2.20	
C_{first}	1.18	3.09	0.00	4.27	–0.27	–0.26	1.71
C_{second}	1.06	3.04	0.00	4.10	–0.10	0.08	2.56
C_{third}	1.07	2.98	0.00	4.05	–0.05	–0.18	2.88
Supercell 6×6	$M_{Total}=4.66\mu_B$						
Mn	0.17	–0.68	5.82	5.31	1.69	2.18	
C_{first}	1.18	3.09	0.00	4.28	–0.28	–0.16	1.71
C_{second}	1.06	3.04	0.00	4.10	–0.10	0.06	2.57
C_{third}	1.07	2.99	0.00	4.06	–0.06	–0.08	2.88
Supercell 7×7	$M_{Total}=2.92\mu_B$						
Mn	0.17	–0.67	5.77	5.28	1.72	0.34	
C_{first}	1.17	3.13	0.00	4.30	–0.30	–0.08	1.72
C_{second}	1.07	3.01	0.00	4.08	–0.08	0.10	2.57
C_{third}	1.06	3.02	0.00	4.08	–0.08	–0.02	2.88
Supercell 8×8	$M_{Total}=4.87\mu_B$						
Mn	0.18	–0.69	5.84	5.33	1.67	2.24	
C_{first}	1.18	3.10	0.00	4.28	–0.28	–0.24	1.72
C_{second}	1.06	3.03	0.00	4.10	–0.10	0.08	2.57
C_{third}	1.07	2.98	0.00	4.05	–0.05	–0.14	2.88

Take the 4×4 and 8×8 supercells for example, their total DOS and PDOS are shown in Figs. 3 and 4. The horizontal axis is energy referring to the Fermi energy. The positive DOS stands for spin up and the negative ones are for spin down electrons. It is well known that the magnetic property originates from asymmetric spin states and thus we mainly discuss the DOS around the Fermi energy. Figure 3(a) plots the DOS of the intrinsic graphene for comparison. As for the 4×4 supercell, from the black curve in Fig. 3(b), it is clear that the total DOS is asymmetric. Several occupied and unoccupied peaks are obviously observed near the Fermi level. Compared with the total DOS of the intrinsic graphene in Fig. 3(a), the empty states near the Fermi level have now developed into four significant peaks for both channels in the Mn-doped graphene. While the intrinsic graphene has few states above 5.0 eV, the doped graphene has zero DOS. The energy states now have well-defined peaks for the spin-up and spin-down electrons with a little shift from their original positions to lower levels. Looking further at Figs. 3(b) and 3(d), a sharp peak of the total DOS appears in the majority channel at −1.0 eV, which certainly originates from the hybridization between C-p and Mn-d orbits, and so is the other sharp peak in the minority channel at 0.3 eV. Besides, there are two peaks, in the majority channel at 0.6 eV and in the minority channel at −0.6 eV, originating from the Mn-3d states. The PDOS of the C-p, Mn-s, and Mn-d electrons are all obviously asymmetric near the Fermi energy, while C-s and Mn-p states are close to linear, or the C-2p and Mn-3d electrons to some extent cause an absence of symmetry in the total spin states. So the magnetic properties mainly stem from the hybridization between C-2p and Mn-3d orbits. This magnetic exchange mechanism occurs in the Mn-doped DSM systems where the Mn orbital electrons are pushed to higher or lower energies, forming different e_g and t_{2g} orbits owing to the Jahn–Teller effect[25] and partially emptied, leading to the hole mediated magnetism, contrasting Fig. 3(c) with Fig. 3(d). These results indicate that the origin of the ferromagnetism in Mn-doped graphene is the p–d exchange mechanism.

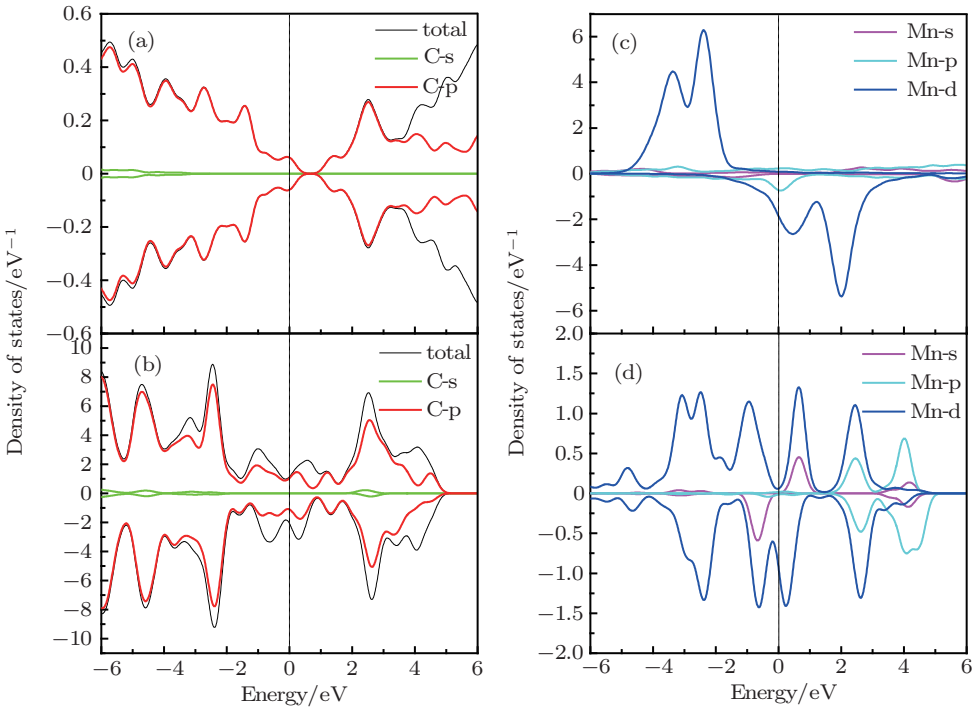


Fig. 3. (color online) Total DOS and PDOS in (a) intrinsic graphene and (b) the 4×4 Mn-doped graphene, (c) the pure Mn metal PDOS, and (d) the Mn atom PDOS in the 4×4 Mn-doped graphene. Black, magenta, cyan, blue, green, and red curves represent the total DOS and the PDOS of Mn-s, Mn-p, Mn-d, C-s, and C-p, respectively.

Interestingly, the minority states of the total DOS show that the system is metallic with some dispersive conduction bands around the Fermi level in the 8×8 Mn-doped graphene supercell as shown in Fig. 4(a). From the PDOS of the Mn atom, we identify the Mn orbits in the vicinity of the band gap region of the pristine graphene (Fig. 3(a)). So the majority channel of the total DOS is semiconducting while the minority one has metallic features. In summary, the 8×8 system has a half metallic structure consistent with the result of Mn adsorption on graphene.[26] The total DOS near the Fermi level is distinctly asymmetric in good agreement with its total magnetic moment in Table 1. It can be seen clearly that the Mn substitution induces the spin splitting impurity states around the Fermi level, forming a small band gap (Fig. 4(c)). The exchange interaction of C-p and Mn-d electrons is situated near −0.9 eV, 1.3 eV, and 2.1 eV, and the peak values of Mn-d states

are consistent with those of C-p states in Figs. 4(b) and 4(c). So the interaction between Mn and C atoms is very strong and the total magnetic moment in the 8×8 supercell is up to 4.8μ_B. The Mn atomic energy band tends toward positions above and below the Fermi energy compared with that of the pure Mn metal (Fig. 3(c)), facilitating the interaction with the C atoms. In addition, the PDOSs of the three nearest C18 and Mn27 are shown in Fig. 4(d), and the C18-2p and Mn-3d electrons undergo sympathetic vibration from −8.0 eV to −1.8 eV. Moreover, there are bonding state peaks near −4.6 eV, −2.4 eV, and 2.2 eV, and anti-bonding states around −2.7 eV and 1.3 eV. The magnetic Mn atom induces the asymmetric electron states of the three C18 atoms around the Fermi energy in good agreement with the −0.24μ_B magnetic moment, which is also the case for the six second nearest C14 atoms and the three third nearest C26 atoms, as shown in Figs. 4(e) and 4(f). The interaction between the Mn atom and the second and the third nearest C atoms produces more anti-bonding orbits, consistent with the bond populations themselves. These neighboring C atoms strongly interact with the Mn atom and obtain magnetic moments of different values, which further indicates the p–d magnetic exchange mechanism. However, there are some hybridized isolated peaks in the low energy level, which shows that these electronic states are hardly affected by the dopant keeping the sp^2 hybridization in Figs. 4(a) and 4(b).

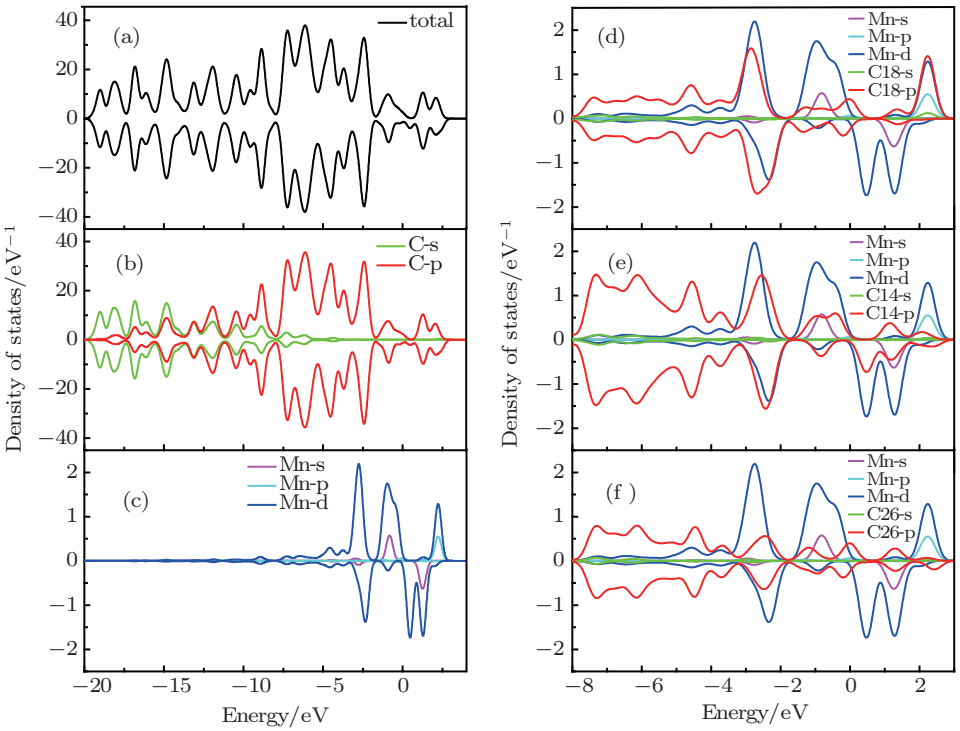


Fig. 4. (color online) (a) Total DOS, the PDOS of (b) C atoms and (c) the Mn atom, and the neighboring (d) C18, (e) C14 and (f) C26 in the 8×8 Mn-doped supercell.

In addition, graphene with one Mn atom doped in a different position is also calculated, showing little effect on the magnetic moment. The same graphene supercell containing two or more Mn atoms is taken into account, and different Mn atom doping is found to have some effect on the magnetic moment and the formation energy. Meanwhile, the different distances between the two Mn atoms in the same size supercell are configured, the results are shown in Table 2. When the two Mn atoms converge (the 7×7-2a state), the total magnetic moment and Mn atomic magnetic moment both are much smaller, owing to fewer C atoms having strong interaction with the Mn atoms. When the distance between the two Mn atoms is longer than a certain length, the magnetic moments of the 7×7-2b, 7×7-2c states are double of that of the 7×7-2a state. However, the formation energy of the 7×7-2a supercell, which is calculated based on the final energy, is approximately 1 eV lower than that of the other two states, so it is a more stable structure. The 7×7-2a system is also more stable than the 7×7 graphene doped by one Mn atom, with 1.12 eV lower formation energy.

Table 2. Final energy (E_{Final}), magnetic moment of each Mn atom (M_{Mn}), total magnetic moment (M_{Total}), and Mn–Mn distance (D_{Mn-Mn}) of the 7×7 supercells with two Mn impurities.

State	M_{Total}	E_{Final}	M_{Mn}	D_{Mn-Mn}
7×7-2a	2.20893	–16179.62400	0.50	1.85512
7×7-2b	5.42409	–16178.70480	1.78	5.68400
7×7-2c	5.36280	–16178.62897	1.78	9.94200

As for the Mn atom, there are 3d electrons inside the 4s shell and the 4s electrons off the Mn ion become the conduction electrons, even 3p electrons. The conduction electrons interact with the 3d ions (Mn^{2+}, Mn^{3+}, or Mn^{4+}) and are in magnetized states. The 3d ions mediated by the magnetized conduction electrons overlap with the C-2p electron cloud and indirectly exchange with each other, leading to the magnetic ordering. In a further quantum explanation of the magnetism in Mn-doped graphene, there is an indirect overlap between the Mn-d and C-p electrons, and the magnetic coupling is therefore determined by the indirect p–d exchange. The indirect coupling between Mn and C atoms thus proceeds through the outer electronic states of the atoms themselves. In the derivation of the Ruderman–Kittel–Kasuya–Yosida (RKKY)[27] exchange, one assumes a δ function-like interaction of a point-like spin $\boldsymbol{S}$, with the spin $\boldsymbol{s}$ of the conduction electrons

$$H = 2A\delta(\boldsymbol{r}-\boldsymbol{R})\boldsymbol{S}\cdot\boldsymbol{s}, \tag{2}$$

where A is the intra-atomic exchange parameter, and the δ function limits the interaction to be of contact form. The RKKY interaction energy between two localized spins $\boldsymbol{S}_i$ and $\boldsymbol{S}_j$ separated by a distance R can then be written in the Heisenberg form

$$H_{eff} = -\sum_{i\neq j}^{N} J_{ij}\boldsymbol{S}_i\cdot\boldsymbol{S}_j = -2\sum_{i<j}^{N} J_{ij}\boldsymbol{S}_i\cdot\boldsymbol{S}_j, \tag{3}$$

with a distance dependent exchange constant $J(R)$. It can be related to the free electron density N_V in-between the atoms. We describe the free electrons as plane waves normalized to a volume V

$$\psi(r) = \frac{1}{\sqrt{V}}\mathrm{e}^{\mathrm{i}\boldsymbol{k}\cdot\boldsymbol{r}}, \tag{4}$$

where the electron momentum $\boldsymbol{k}$ is related to the electron kinetic energy by the free electron dispersion relation

$$E = \frac{\hbar^2\boldsymbol{k}^2}{2m_\mathrm{e}}. \tag{5}$$

The total density of states per unit energy, including two spins per unit energy, is obtained by counting the number of states in the volume V per unit energy and is given by

$$D(E) = \frac{V}{\pi^2\hbar^2}m_\mathrm{e}k = \frac{V}{2\pi^2\hbar^3}(2m_\mathrm{e})^{3/2}\sqrt{E}. \tag{6}$$

If we denote the electron density per unit volume as N_V, the total number of electrons in volume V is $N_V V$. By equating $N_V V$ with the energy integral of Eq. (6) up to the Fermi energy, we obtain

$$N_V = \frac{1}{V}\int_0^{E_\mathrm{F}} D(E)\,\mathrm{d}E = \frac{(2m_\mathrm{e}E_\mathrm{F})^{3/2}}{3\pi^2\hbar^3} = \frac{k_\mathrm{F}^3}{3\pi^2}, \tag{7}$$

where the Fermi energy E_F and Fermi wave vector k_F are related according to $E_\mathrm{F} = \hbar^2k_\mathrm{F}^2/2m_\mathrm{e}$. The RKKY exchange coefficient $J(R)$ is found to be oscillatory with distance R according to

$$J(R) = \frac{16A^2m_\mathrm{e}k_\mathrm{F}^4}{(2\pi)^3\hbar^2}\left[\frac{\cos(2k_\mathrm{F}R)}{(2k_\mathrm{F}R)^3} - \frac{\sin(2k_\mathrm{F}R)}{(2k_\mathrm{F}R)^4}\right]. \tag{8}$$

It makes a damped oscillation with distance from positive to negative, which at large R takes the simple form[28]

$$J(R) = \frac{2A^2m_\mathrm{e}k_\mathrm{F}}{(2\pi)^3\hbar^2}\frac{\cos(2k_\mathrm{F}R)}{R^3} \sim \frac{1}{R^3}. \tag{9}$$

Therefore, depending upon the separation between the magnetic ions, their magnetic interaction can be either ferromagnetic or antiferromagnetic. The RKKY exchange couples have localized moments over relatively large distances. Furthermore, the density of the spin-up and -down conduction electrons decays in an oscillatory way with the distance $|r-R|$ off the ion,[29] and so is the Mn-doped graphene. With increasing distance from the manganese ion, the polarization of carbon atoms attenuates.

4. Conclusion

In this paper, the ferromagnetic property of graphene-based DMS is investigated by Mn doping using first-principles calculations. It is found that Mn-doped graphene has strong ferromagnetism and the magnetic moment varies with the dopant concentration. Moreover, the 8×8 Mn-doped graphene of a single impurity possesses the greatest magnetic moment, and the 7×7 supercell doped by two converged Mn atoms is more stable. Finally, we give an RKKY explanation for the p–d indirect exchange of the magnetic ordering.

References

[1] Novoselov K S, Geim A K, Morozov S V, Jiang D, Zhang Y, Dubonos S V, Grigorieva I V and Firsov A A 2004 *Science* **306** 666
[2] Han M Y, Özyilmaz B, Zhang Y B and Kim P 2007 *Phys. Rev. Lett.* **98** 206805
[3] Rycerz A, Tworzydlo J and Beenakker C W J 2007 *Nat. Phys.* **3** 172
[4] Xu J M, Hu X H and Sun L T 2012 *Acta Phys. Sin.* **61** 027104 (in Chinese)
[5] Wehling T O, Katsnelson M I and Lichtenstein A I 2008 *Appl. Phys. Lett.* **93** 202110
[6] Leenaerts O, Partoens B and Peerers F M 2008 *Phys. Rev. B* **77** 125416
[7] Wu M, Liu E Z, Ge M Y and Jiang J Z 2009 *Appl. Phys. Lett.* **94** 102505
[8] Dai X Q, Tang Y N, Zhao J H and Dai Y W 2010 *J. Phys.: Condens. Matter* **22** 316005
[9] Dedkov Y S, Shikin A M, Adamchuk V K, Molodtsov S L, Laubschat C, Bauer A and Kaindl G 2001 *Phys. Rev. B* **64** 35405
[10] Ohno Y, Young D K, Beschoten B, Matsukura F, Ohno H and Awschalom D D 1999 *Nature* **402** 790
[11] Bhattacharya A, Bhattacharya S, Majumder C and Das G P 2010 *J. Phys. Chem. C* **114** 10297
[12] Nemnes G A 2012 *J. Nanomaterials* **2012** 748639
[13] Hu X H, Xu J M and Sun L T 2012 *Acta Phys. Sin.* **61** 047106 (in Chinese)
[14] Eelbo T, Waśniowska M, Thakur P, Gyamfi M, Sachs B, Wehling T O, Forti S, Starke U, Tieg C, Lichtenstein A I and Wiesendanger R 2013 *Phys. Rev. Lett.* **110** 136804

[15] Geim A K and Novoselov K S 2007 *Nat. Mater.* **6** 183
[16] Hohenberg P and Kohn W 1964 *Phys. Rev.* **136** B864
[17] Kohn W and Sham L J 1965 *Phys. Rev.* **140** A1133
[18] Perdew J P, Burke K and Ernzerhof M 1996 *Phys. Rev. Lett.* **77** 3865
[19] Pfrommer B G, Cote M, Louie S G and Cohen M L 1997 *J. Comput. Phys.* **131** 233
[20] Blöchl P E 1994 *Phys. Rev. B* **50** 17953
[21] Kresse G and Joubert D 1999 *Phys. Rev. B* **59** 1758
[22] Gorjizadeh N and Kawazoe Y 2008 *Materials Transactions* **49** 2445
[23] Wu M, Cao C and Jiang J Z 2010 *New J. Phys.* **12** 063020
[24] Santos E J G, Ayuela A and Sánchez-Portal D 2010 *New J. Phys.* **12** 053012
[25] Seman T F, Ahn K H, Lookman T, Saxena A, Bishop A R and Littlewood P B 2012 *Phys. Rev. B* **86** 184106
[26] AlZahrani A Z 2012 *Physica B* **407** 992
[27] Stöhr J and Siegmann H C 2010 *Magnetism* (Beijing: World Publishing Company) pp. 290–292
[28] Nolting W and Ramakanth A 2009 *Quantum Theory of Magnetism* (New York: Springer Heidelberg Dordrecht New York) pp. 207–209
[29] Jin H Q 2013 *Magnetic Physics* (Beijing: Science Press) pp. 84–90 (in Chinese)